Article

Not peer-reviewed version

Numerical Simulation and Modeling of Mechano–Electro–Thermal Behavior of Electrical Contact Using COMSOL Multiphysics

Andrei Andras *, Florin Dumitru Popescu *, Sorin Mihai Radu, Dragos Pasculescu, Ildiko Brinas, Mirela Ancuta Radu, Daniela (Furdui) Peagu

Posted Date: 25 March 2024

doi: 10.20944/preprints202403.1416.v1

Keywords: electrical contact; Joule heating; Thomson effect; simulation; COMSOL Multiphysics; current density; electrical contact temperature.

Article

Numerical Simulation and Modeling of Mechano–Electro–Thermal Behavior of Electrical Contact Using COMSOL Multiphysics

Andrei Andras [1,*], Florin Dumitru Popescu [1,*], Sorin Mihai Radu [1], Dragos Pasculescu [2], Ildiko Brinas [1], Mirela Ancuta Radu [3] and Peagu (Furdui) Daniela [4]

[1] Department of Mechanical, Industrial and Transport Engineering (IMIT), University of Petroșani, 332006 Petroșani, Romania; sorin_mihai_radu@yahoo.com (S.M.R.); kerteszildiko@ymail.com (I.B.)
[2] Department of Automatics, Computers, Electrical and Energetics Engineering (ACIEE), University of Petroșani, 332006 Petroșani, Romania; dragospasculescu@upet.ro
[3] National Institute of Research and Development for Safety in Mines and Explosion Protection—INSEMEX Petrosani, 332047 Petrosani, Romania; mirela.radu@insemex.ro
[4] Doctoral School in Mines, Oil and Gases, University of Petrosani, 332006 Petrosani, Romania; danafurdui2012@yahoo.com
* Correspondence: andrei.andras@gmail.com (A.A.); fpopescu@gmail.com (F.D.P.)

Abstract: Electrical contacts are important circuit components with diverse industrial applications, and their failure can lead to multiple unwanted effects. Hence, the behavior of electrical contacts is a widely studied topic in scientific literature based on various approaches, tools, and techniques. The present study proposes a numerical modeling and simulation approach based on the Holm contact theory to study the dependence between the electric potential and the temperature within an electrical contact. Structured in 5 sections, the research was conducted using COMSOL Multiphysics software and its solid-state mechanics, electric current, and heat transfer modules in order to highlight contact behavior from mechanical, electrical and thermal points of view: the von Mises stress, contact force, the electric field amplitude, the variation of the electrical potential along the current path, the temperature gradient, and dependence of temperature along the contact elements edges were obtained by simulation and graphically represented. The results are in line with the expectations and with past research that was studied in the literature review.

Keywords: electrical contact; joule heating; Thomson effect; simulation; COMSOL multiphysics; current density; electrical contact temperature

1. Introduction

Electrical contacts are crucial circuit components present in most electric devices, such as relays, switches, breakers, connectors, breakers and integrated circuits. The theory and analysis of electrical contacts [1–5] is a multidisciplinary issue since it involves electrical, mechanical and thermal concepts, all aimed at understanding and improving the performance of these electrical connections used in various applications.

A contact system always consists of a pair of electric contacts and a source of contact force [6], with each contact made of conductive material, usually metal or metallic alloys. When a pair of contacts touch, electrical current passes with a certain electrical contact resistance. There are several factors [7] that influence the current flow and thus this resistance: contact area [8], shape [9], roughness [10], oxidation and coatings [11,12], mechanical loads [13], etc. The electrical contacts' resistance should be low and stable, since its increase leads to contact failure and very high Joule heat losses [14].

 doi:10.20944/preprints202403.1416.v1

The typical failure modes for electrical contacts consist of: (a) temperature increase in the contact area producing melting or quick aging, (b) elevated electrical contact resistance caused by fretting wear or oxidation, and (c) excessively small or large closing/opening forces.

Failures of electrical contacts and the causes leading to them are extensively studied in the scientific literature, based on several different analysis approaches.

First, there are theoretical analyses based on model types such as the single point (or Holm tube) contact model [15,16], the multi-point contact model [17,18], or the fractal geometry theory model [19–21]. A number of several other scholars used analytical models to study electrical contact behavior with authors of [22] presenting a study built on the improved elastic rough surface model, [23] introducing a new analytical model for the analysis of switching devices contact area for different voltage and current magnitudes and [24] proposing a semi-analytical model based on the single asperity concept to highlight the flow of current between two contacting surfaces.

Next, electrical contacts have been also widely studied using experimental setups and measurements, employing a combined analytical and experimental investigation [25] to describe the electrical-thermal behavior of electrical contact systems, using a low-cost tabletop indenter setup [26] to measure the in-situ electrical contact resistance, determining experimentally the adhesion force and energy at contact interfaces for conductive, isotropic, and rough surfaces [27]. High current automotive connectors were tested [28] to assess their thermal performance, experimental observations on contact resistance were summed up [29] to be used as an electrical contact guide, two distinct techniques were used during investigations [30] for different pressures, temperatures, and contact types, and trials were conducted [31] on copper/brass plug-and-sockets type of contacts.

Finally, there are the vast array of numerical methods. These started several decades ago with finite elements discretization [32,33] and solving in codes like FEAP [34–36] or discrete elements simulations using the LMGC90 open platform or MULTICOR software [37–40] but in the recent years the continuous advance of computer technology and the leap in performance and processing power allows to model, analyze, optimize and solve more and more complex problems of electrical contact systems. Nowadays, the numerical methods use dedicated engineering computer software, and are based on various techniques such as the boundary element method (BEM) [41–43], finite element method (FEM) [44–46] or coupled/multiphysics methods [47–49] to model and simulate contact behavior.

Angadi et al. [50] and other scholars reviewed and presented several computer software available to researchers for the analysis of electrical contacts and their behavior, with MSC Marc, ANSYS, ABAQUS and COMSOL being the most used ones as subsequently detailed:

(a) MSC Marc software was used in [51] to create the model of an electric contact and compute the temperature distribution of joule heating compared with experimental results. The performance of pin and socket electrical contacts was assessed in [52] using a computer model developed also in MSC Marc software and numerical simulation;

(b) ANSYS was used by Duan et al. [53] to develop a coupled mechanical–electrical–thermal model, in order to prove the relation between electric contact shrink range, contact resistance and maximum stress also considering the temperature. Authors of [54] proposed a multi-physics model developed in ANSYS to investigate the thermal behavior of an electrical contact with rough surface in two scenarios: direct and load transfer. The model developed introduced in [55] combines ANSYS with a MATLAB code to accurately predict the contact forces, thermal contact resistance, surface separation and ECR and provide an efficient tool to study electrical contact behavior from electrical, thermal and structural perspective;

(c) ABAQUS and FE-SAFE software are both used [56] to numerically investigate and assess in detail the behavior of aviation electrical contacts. Authors of [57] use an ABAQUS developed thermal-electric coupled simulation to study the contact pair insertion force and obtain the contact resistance. A analysis was conducted using a new electro-thermo-mechanical contact model developed by [58] in ABAQUS and two user-defined subroutines to show how the contact state significantly influences the local heating;

 doi:10.20944/preprints202403.1416.v1

(d) Finally, the Swedish COMSOL Multiphysics software is used by Zhang et al. [59] to introduce a new fluid-solid heat transfer model coupled with contact mechanics and thermo-electric effect, in order to highlight the importance of the pressure on the failure of an electrical contact. Another COMSOL developed model is proposed in [60] to conduct research on the contact temperature characteristics in order to improve the performance of electrical contacts. Authors of [61] investigate by simulation in COMSOL of the effects of the electric current and contact force on the temperature and resistance of a spring type electrical contact.

However, regardless of the method applied or the software used all have both limitations and advantages, so at this point there is no imposed standard requiring a particular computer program or method of analysis. Taking this into consideration, given the extensive literature review pointing to the available software tools, and considering the experience and previous approaches [62–65] of the same research team in solving various engineering tasks using numeric simulation, in the present study COMSOL software [66] was chosen for the analysis and SolidWorks for the creation of the geometric model.

The purpose of the present paper is to develop a modeling approach based on Holm electrical contact theory in order to investigate the dependance between the electric potential and the temperature of the electrical contact by numerical methods using the COMSOL software and FEM. The results obtained are in line with the expectations and with past research presented in the literature review section.

The paper is structured as follows: Section 1 introduces the purpose if the paper and presents a comprehensive literature review on the studied thematic, Section 2 presents the theoretical aspects regarding electric contacts. Section 3 shows the initial geometric model development using SolidWorks software, followed by the step-by-step creation of the COMSOL model and the simulation studies run in the same software, and section 4 discusses the results obtained.

2. Theoretical Considerations about Electrical Contacts

As described in the Introduction section, an electrical contact consists of a pair of usually metallic contact elements, by the touch of which conduction in an electrical circuit is established. In practice, the touching of the two elements is achieved by pressing one element against the other by means of a force. This contact force can be produced by either springs (by compression or stretching) or bolts that mechanically join the two elements. In order to study and express contact behavior in mathematical formulae, it is necessary to know the main physical processes that occur when forming an electrical contact. One can imagine a simple experiment: two straight metal cylinders with similar cross section and very finely polished end surfaces are pressed against each other with a force F, as shown in Figure 1. If the measured resistance R_m along the length comprising the junction of elements l is compared with the resistance value calculated as $R_c = \rho \cdot l / A$ where l is the length, A is the transversal cross-section of the cylinders and ρ is the material resistivity, it is found that $R_c << R_m$. The explanation for this lies in the constriction of current lines of flow, and in the formation of a disturbing film on the processed surfaces.

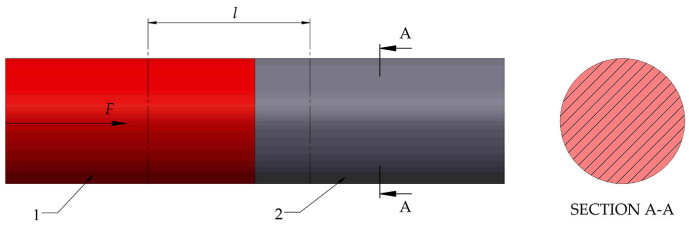

Figure 1. Contact between two metallic cylinders with similar section.

 doi:10.20944/preprints202403.1416.v1

No matter how finely the contact surfaces are polished, the actual touch is achieved only in certain areas called contact points, where the current lines of flow are bent and undergo a constriction as shown in Figure 2. Also, the surfaces of contact elements react with the atmosphere forming a film of Cu_2O on copper surfaces and Ag_2S on silver ones which also increases contact resistance.

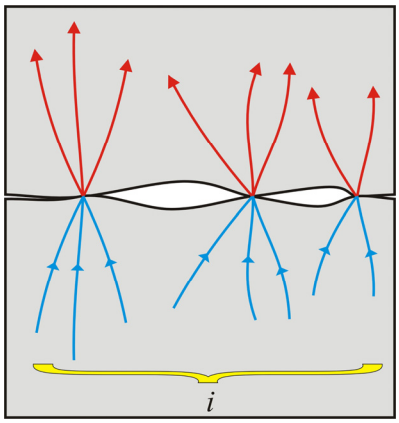

Figure 2. Constriction of the current lines of flow.

In contacts with a large area the effective contact area is smaller as compared to the apparent touching area, because surfaces that appear smooth at real scale are actually rough and contaminated at microscopic scale [67]. The contact elements actually touch in micro-points of contact which are grouped into contact areas that are called contact spots or a-spots where, where the material is deformed. If the area of contact points A_F on which the contact force F is exerted is only a tiny fraction (0.01—0.05) of the apparent area A_a, there is a surface contact as illustrated in Figure 3 where contact is achieved through three a-spots noted 1, 2, and 3.

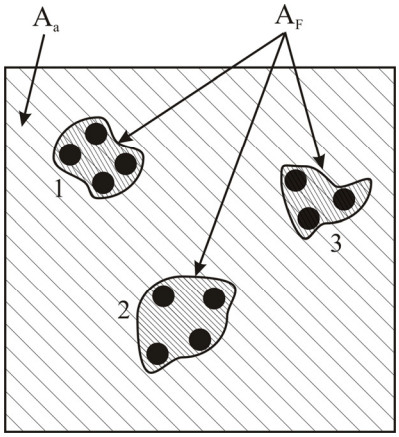

Figure 3. Surface contact illustration of effective and actual contact area.

Each contact spot consists of micro-areas where the material is deformed either plastically, elastically or both. The dependence between the contact force F and the contact area A_F on which this force is exerted under plastic deformation conditions can be expressed using the formula of Holm [68]:

$$A_F = \frac{F}{\xi \cdot H} = n \cdot \pi \cdot a^2 \quad (1)$$

where a is the radius of the equivalent circle for each of the n contact zones.

 doi:10.20944/preprints202403.1416.v1

Equation (1) shows that the magnitude of the contact area does not depend on the contact force, but only on the hardness of the material H and coefficient ξ. This coefficient is subunitary and was introduced in the equation to mark that the hardness of the contact peaks is less than the hardness H measured macroscopically by pressing a sphere against a flat surface. If the touch between the two elements is achieved through a single contact area, a single-point contact is obtained. In practice this can be achieved by means of an element including a spherical cap and an element including a flat surface, as shown in Figure 4. In this case the dependence between the contact area $\pi \cdot a^2$ and the contact force F is:

$$A_F = \pi \cdot a^2 = \frac{F}{H} \tag{2}$$

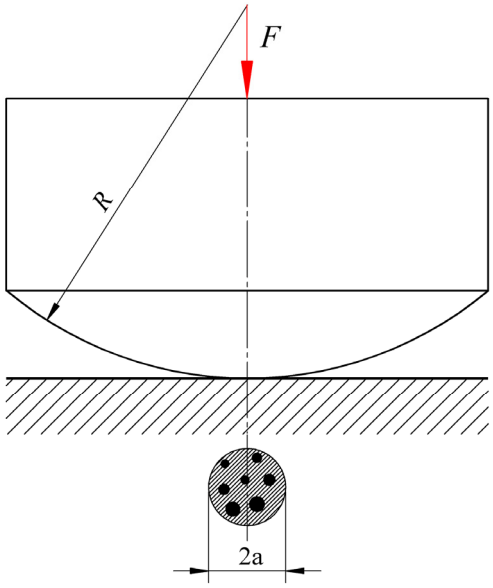

Figure 4. The single-point contact illustration.

Equation (2) does not include a dependence between the contact area and the radius of the contact element in the field of plastic deformation where technical contacts belong.

For the calculation of the constriction resistance two models can be applied [69], namely, the infinite conductivity sphere model and the flattened ellipsoid model.

2.1. The Model of the Infinite Conductivity Sphere

The model of the infinite conductivity sphere shown in Figure 5 consists of two half-spaces 1 and 2 of finite conductivity which model the contact elements, where the electrical conduction is established by means of a sphere of radius a and infinite conductivity. The current lines are radial, and the equipotential surfaces are spherical. The current density is constant over the surface of a sphere of radius r.

 doi:10.20944/preprints202403.1416.v1

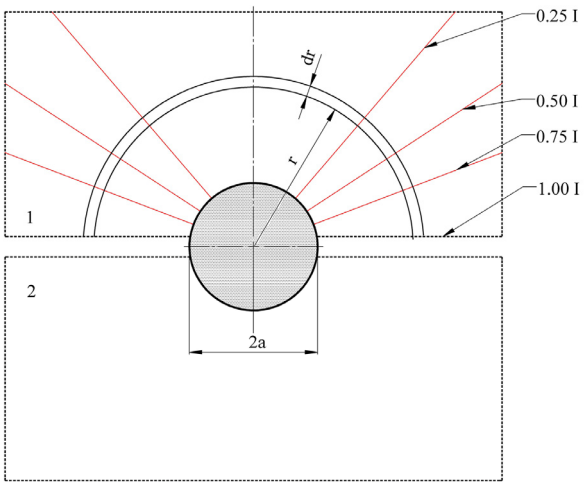

Figure 5. The model of the infinite conductivity sphere.

If ρ is the resistivity of the material of the half-spaces, the elementary resistance is:

$$\mathrm{d}R_s = \frac{\rho \mathrm{d}r}{2\pi r^2} \tag{3}$$

and by integration the constriction resistance of one half-space becomes:

$$R_s = \frac{\rho}{\pi}\int_a^{\infty}\frac{\mathrm{d}\,r}{r^2} = \frac{\rho}{2\pi a} \tag{4}$$

The total contact constriction resistance of the two half-spaces in touch with the infinite conductivity sphere having a diameter 2*a*, is twice the value given by Euation (4), i.e.,:

$$R = \frac{\rho}{\pi a} \tag{5}$$

2.2. The Flattened Ellipsoid Model

In the case of the flattened ellipsoid model, the half-spaces 1 and 2 of finite conductivity are touching by means of a flattened ellipsoid, as shown in Figure 6. The equipotential surfaces are confocal ellipsoids, with the flattened ellipsoid as their base ellipsoid. To calculate the electrical resistance between the equipotential surface of the base ellipsoid (as a place of contact) and the surface of another equipotential confocal ellipsoid, formal analogy is used, which exists between the formulae characterizing the stationary electric field of direct current in a conducting medium and the formulae characterizing the electric field in an uncharged dielectric.

 doi:10.20944/preprints202403.1416.v1

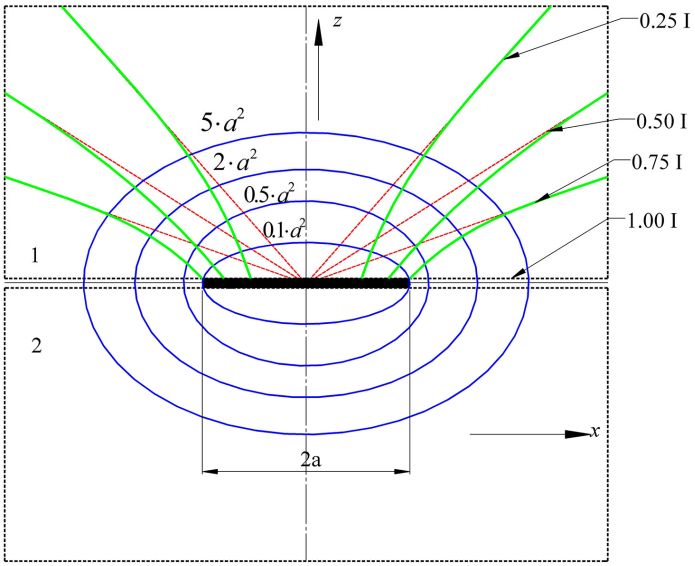

Figure 6. The flattened ellipsoid model.

In this case, the expression of striction conductance is identical to the expression of capacitance in which permittivity ε is replaced by conductivity σ. Solving the problem in this way is possible assuming the same boundary conditions are allowed for both the conductive medium with conductivity σ and the dielectric medium with permittivity ε. Thus, both the base ellipsoid and the medium delimiting the surface of the confocal ellipsoid are assumed to have infinite conductivity, and the conductive medium between the surfaces of the ellipsoids has constant conductivity σ. Only in this case are the surfaces of the two ellipsoids equipotential surfaces in the stationary electric field, and the current lines are orthogonal to the surfaces of the ellipsoids.

If it is considered that the base ellipsoid is flattened as in Figure 6, and that the contact surface is an ellipse, then the equipotential surfaces in the contact members are semi-ellipsoids with the equation:

$$\frac{x^2}{\alpha^2+\mu}+\frac{y^2}{\beta^2+\mu}+\frac{z^2}{\mu}=1 \tag{6}$$

where α and β are the semi-axes of the flattened base ellipsoid in the plane xy. Confocal ellipsoids are defined by the parameter μ ($\mu=0.1\cdot a^2$, $\mu=0.5\cdot a^2$, $\mu=2\cdot a^2$, $\mu=5\cdot a^2$, ...). Thus, the semi-axes are: $\sqrt{\alpha^2+\mu}$ on axis x, $\sqrt{\beta^2+\mu}$ on axis y, and $\sqrt{\mu}$ on axis z.

The capacitance between the base ellipsoid and a confocal ellipsoid is:

$$C=\frac{8\pi\varepsilon}{\int_0^{\mu}\frac{d\mu}{\sqrt{(\alpha^2+\mu)(\beta^2+\mu)\mu}}} \tag{7}$$

and the capacitance between the base semi-ellipsoid and a confocal semi-ellipsoid is:

$$C_s=\frac{4\pi\varepsilon}{\int_0^{\mu}\frac{d\mu}{\sqrt{(\alpha^2+\mu)(\beta^2+\mu)\mu}}} \tag{8}$$

Based on the afore mentioned analogy, the constriction resistance between the base semi-ellipsoid and a random confocal semi-ellipsoid is:

 doi:10.20944/preprints202403.1416.v1

$$R_s = \frac{1}{4\pi\sigma}\int_0^{\mu}\frac{\mathrm{d}\mu}{\sqrt{\left(\alpha^2+\mu\right)\left(\beta^2+\mu\right)\mu}} \tag{9}$$

If it is admitted that the contact ellipse is actually a circle, meaning that $\alpha = \beta = a$ then the elliptical integral becomes a simple transcendent integral, and:

$$R_s = \frac{1}{4\pi\sigma}\int_0^{\mu}\frac{\mathrm{d}\mu}{\left(a^2+\mu\right)\sqrt{\mu}} \tag{10}$$

With the variable changes $\sqrt{\mu} = z$, $\mu = z^2$, and $d\mu = 2z\,dz$ we obtain:

$$R_s = \frac{1}{2\pi\sigma}\int_0^{\sqrt{\mu}}\frac{\mathrm{d}\,z}{a^2+z^2} = \frac{1}{2\pi\sigma a^2}\int_0^{\sqrt{\mu}}\frac{\mathrm{d}\,z}{1+\left(\frac{z}{a}\right)^2} \tag{11}$$

With a new variable change $\frac{z}{a} = u$, $dz = a\cdot du$ we obtain:

$$R_s = \frac{1}{2\pi\sigma a}\int_0^{\frac{\sqrt{\mu}}{a}}\frac{\mathrm{d}\,u}{1+u^2} = \frac{\rho}{2\pi a}\arctan\left(\frac{\sqrt{\mu}}{a}\right) \tag{12}$$

If instead of an ellipsoid a semi-space is considered then $\mu\to\infty$, and Equation (12) becomes:

$$R_s = \frac{\rho}{4a} \tag{13}$$

The total constriction resistance is twice as high as R_s:

$$R = \frac{\rho}{2a} \tag{14}$$

According to Holm [67], the current density across a flattened ellipsoid contact area can be approximated as:

$$J(r) = \frac{i}{2\pi a}\cdot\frac{1}{\sqrt{a^2-r^2}} \tag{15}$$

The analysis of the structure of electrical contacts which have bonded due to the current passing through them, shows that soldering and therefore melting of the material occurs at the edge of the point contact which justifies the acceptance of the flattened ellipsoid as a calculation model. In Figure 5 of the infinite conductivity sphere, the current lines of flow for 0.25 I, 0.5 I, 0.75 I, and I were plotted. It is found that at $\mu=0.5\cdot a^2$ the confocal ellipsoid comes very close to a sphere, and at $\mu=20\cdot a^2$ it is practically similar to a sphere. For this situation, the distance to the flattened ellipsoid is $z = \sqrt{\mu} = 4.472\cdot a$, and the semi-axis after the axis x is $\sqrt{a^2+\mu} = 4.582\cdot a$.

Knowledge of the dependence between the contact force and electrical resistance provides a first criterion for the dimensioning of electrical contacts. For a point contact in the case of elastic deformation, the contact area between two spheres or two cylindrical bars is calculated using Hertz's formula:

$$a = \sqrt[3]{\frac{3}{4}\cdot F\cdot\left(\frac{1-\sigma_1^2}{E_1}+\frac{1-\sigma_2^2}{E_2}\right)\cdot\left(\frac{1}{r_1}+\frac{1}{r_2}\right)^{-1}} \tag{16}$$

where the notations (according to Figure 7a,c) are: a – radius of circular contact surface; F – the contact force; σ_1, σ_2 –Poisson's ratio for both elements of the contact; E_1, E_2 – the corresponding modulus of elasticity; r_1, r_2 –the corresponding radii of the two spheres.

 doi:10.20944/preprints202403.1416.v1

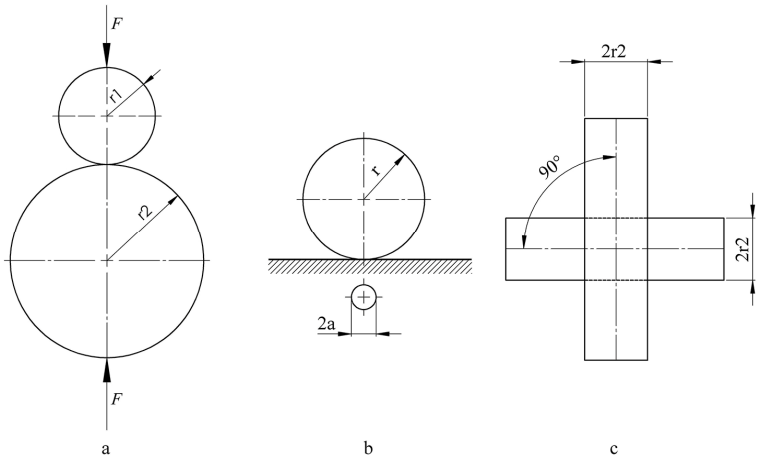

Figure 7. Contacts under elastic deformations condition.

In the case of a contact between a sphere with the radius $r_1 = r$ and a plane $r_2 = \infty$, as shown in Figure 7b., and the material in both contact elements is the same ($\sigma_1 = \sigma_2 = \sigma$, $E_1 = E_2 = E$) then Equation (16) becomes:

$$a = \sqrt[3]{1,5\left(1-\sigma\right)^2 \frac{F \cdot r}{E}} \tag{17}$$

or, for r, σ and E assumed constant it can be expressed as:

$$a \approx \sqrt[3]{F} \tag{18}$$

The dependence between the contact resistance and contact force results:

$$R = \frac{\rho}{2a} \approx \sqrt[3]{F} \tag{19}$$

Consequently, in the case of plastic deformation, the radius of the contact circle is:

$$a = \sqrt{\frac{F}{\pi H}} \tag{20}$$

and the dependence is:

$$R = \frac{\rho}{2a} = \frac{\rho}{2}\sqrt{\frac{\pi H}{F}} = \frac{1}{\sqrt{F}} \tag{21}$$

Technical contacts usually employ plastic deformation. Equation (21) does not show a dependence of resistance on the curvature of the contact, but highlights the fact that the contact resistance is inversely proportional to the contact force at a fractional power. Experience shows that there is a dependence of the contact resistance on the radius of the contact element on silver coated copper contacts.

2.3. The Thermal Regime of Electrical Contacts

From the point of view of the thermal regime of electrical contacts, electric current passing through a contact causes the development of heat (Joule effect) because of contact resistance. In permanent thermal regime, the overtemperature due to contact resistance must be maintained within relatively low limits of 2–10 degrees, whereas in short-term thermal regime such as short-circuit, the overtemperature must not lead to melting of the contact elements. Studying of thermal behavior is carried out for closed contacts, as if the contact elements are separated, additional physical processes such as arcing and material migration occur.

 doi:10.20944/preprints202403.1416.v1

Figure 8 shows a contact point in whose touching area a number of m flow lines (tubes) of current i converge, such that the total current in the touch area is $I = m \cdot i$. Figure 9 schematically details such a tube of current, which in the contact point covers the area ΔA_0.

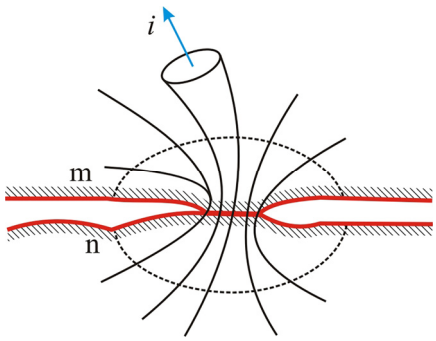

Figure 8. Contact point with converging flow lines (tubes) of current.

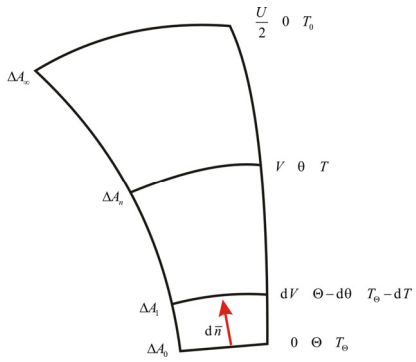

Figure 9. Detailed view of a tube of current.

Calculations are made with the following assumptions:

- The thermal flux developed in a certain current tube is transmitted outwards only through that current tube. There is no heat transfer between adjacent points m and n in Figure 8, which are assumed to be at the same temperature;
- The highest overtemperature is at ΔA_0 surface, which also defines an isothermal surface, as a result of which the greatest striction is located in the contact zone;
- The contact elements are made of the same homogeneous and isotropic material.

By the passing of current i through a current tube, equipotential and isothermal surfaces are defined as shown in Figure 9, considering the surface ΔA_2 with the reference parameters in terms of electric potential $V = 0$, overtemperature $\theta = \Theta$, and absolute temperature $T = T_\Theta$. A surface ΔA_n located far, theoretically at infinity is characterized by $V = U/2$, where U is the voltage on the contact, $\theta = 0$ and $T = T_0$.

One can notice that the equipotential surfaces are also isothermal, due to the fact that equal thermal fluxes go through equal thermal resistances. Thus, the equations of electrical resistance R and thermal resistances R_t, for a segment of the current tube between the base surface ΔA_0 and the equipotential surface ΔA_1 situated at a distance d n from ΔA_0 are:

$$\mathrm{d}\,R = \frac{\mathrm{d}\,n}{\sigma \cdot \Delta \bar{A}_{01}} \tag{22}$$

$$\mathrm{d}\,R_t = \frac{\mathrm{d}\,n}{\lambda \cdot \Delta \bar{A}_{01}} \tag{23}$$

 doi:10.20944/preprints202403.1416.v1

where $\Delta\overline{A}_{01}$ represents an average value of the area over the distance d n; σ is the electrical conductivity; λ is the thermal conductivity.

For the elementary temperature variation, the equation of Fourier is valid written in the form:

$$\mathrm{d}\,T = -P_t \cdot \mathrm{d}\,R_t \tag{24}$$

where P_t is the thermal power and d R_t the thermal resistance traveled by the thermal power. To integrate the differential Equation (24) based on Equations (22) and (23) one can write:

$$\mathrm{d}\,R_t = \mathrm{d}\,R\,\frac{\sigma}{\lambda} = \frac{\mathrm{d}\,R}{\lambda\rho} \tag{25}$$

which can also be expressed as:

$$\mathrm{d}\,R = \frac{\mathrm{d}\,V}{i} \tag{26}$$

Under these conditions, Equation (25) becomes:

$$-\lambda\rho\,\mathrm{d}\,T = V\,\mathrm{d}\,V \tag{27}$$

Equation (27) allows to express the dependence between the absolute temperature of the contact and the electrical potential, of the form:

$$-\int_{T_\Theta}^{T} \lambda\rho\,\mathrm{d}\,T = \int_0^V V\,\mathrm{d}\,V \tag{28}$$

To solve Equation (28), λ and ρ are considered as functions of temperature. Two cases can exist, namely:

(a) The overtemperature is moderate, i.e., Θ = 1... 5 degrees. In this case, the product $\lambda\rho$ may take an average value $\overline{\lambda\rho}$. Thus, by integrating Equation (28) we obtain:

$$T_\Theta - T = \theta_\Theta - \theta = \frac{V^2}{2\overline{\lambda\rho}} \tag{29}$$

and if the integration is done for a remote area, the contact overtemperature is obtained:

$$T_\Theta - T = \Theta = \frac{U^2}{8\overline{\lambda\rho}} \tag{30}$$

(b) The overtemperature is excessive, meaning that the material tends to melt. In this case, the Wiedemann-Franz-Lorenz law is used:

$$\lambda\rho = LT \tag{31}$$

By integrating within limits T_Θ, T_0 and, respectively 0, U/2 the Equation (28) it results that:

$$L\left(T_\Theta^2 - T_0^2\right) = \frac{U^2}{4} \tag{32}$$

The temperature field of the current paths in which there are contacts is obtained taking into account the permanent end effect, and has the expression:

$$\theta = \left(\theta^* - \theta_{\max}\right)\mathrm{e}^{-\beta x} + \theta_{\max} \tag{33}$$

For the determination of θ^* it is observed that the contact resistance is actually a narrow-place (constriction) resistance and that half of the electrical power developed by the contact resistance is injected into the front surface of the contact, i.e.,:

$$\frac{Ri^2}{2} = \frac{P}{2} = -\lambda A\left(\frac{\partial\theta}{\partial x}\right)_{x=0} \tag{34}$$

 doi:10.20944/preprints202403.1416.v1

From Equation (33) the temperature gradient at the contact site can be calculated:

$$\left(\frac{\partial\theta}{\partial x}\right)_{x=0} = -\beta\left(\theta^* - \theta_{\max}\right) \tag{35}$$

so that from (35) the overtemperature of the frontal surface is obtained:

$$\theta^* = \frac{P}{2\lambda A\beta} + \theta_{\max} \tag{36}$$

Note that the equation above has two components, namely θ_c representing the contribution of contact:

$$\theta c = \frac{P}{2\lambda A\beta} = \frac{Ui}{2\lambda A\beta} \tag{37}$$

and θ_{max} which is the contribution of the conductor traveled by the current in permanent mode. This means that the contact overtemperature is given by (37) as a function of the power developed by the contact resistance, which implies knowing the voltage U of the contact.

The resistance of the unheated contact (an electric current of zero intensity flows though the contact) differs from the resistance of the heated contact (an electric current of significant intensity flows though it). The dependence between the electrical resistance R_Θ of the heated contact and the electrical resistance R_0 of the unheated contact can be determined using the theory of electric potential. With reference to this, two strictions are considered, namely: striction $S(\lambda,\rho)$, where λ and ρ depend on temperature and, striction $S_0(\lambda_0,\rho_0)$, where λ_0 and ρ_0 do not depend on temperature. For the two strictions the elementary variation of potential can be expressed as:

$$\mathrm{d}V = \rho\frac{\mathrm{d}n}{\Delta A_n}\mathrm{i}; \quad \mathrm{d}V_0 = \rho_0\frac{\mathrm{d}n}{\Delta A_n}i \tag{38}$$

Since the dependence of resistivity on temperature is of the form $\rho = \rho_0(1+\alpha_R\theta)$, from Equation (38) it can be written that $\mathrm{d}V = \mathrm{d}V_0(1+\alpha_R\theta)$, and thus:

$$\mathrm{d}V_0 = \mathrm{d}V\left(1-\alpha_R\theta\right) \tag{39}$$

In this case, Equation (28) can be also written as:

$$-\int_\Theta^\theta \overline{\lambda\rho}\,\mathrm{d}\theta = \int_0^V V\,\mathrm{d}V$$

which becomes, after integration:

$$\theta = \Theta - \frac{1}{2}\cdot\frac{V^2}{\lambda\rho} \tag{40}$$

where, according to (30), $\Theta = \frac{U^2}{8\overline{\lambda\rho}}$.

Equation (39) with the expression of θ introduced from Equation (40) is integrated within limits Θ, 0 for the heating and 0, $U/2$ for the potential:

$$\int_0^{\frac{U_0}{2}}\mathrm{d}V_0 = \int_0^{\frac{U}{2}}\mathrm{d}V - \int_0^{\frac{U}{2}}\left(\alpha_R\Theta - \frac{\alpha_R V^2}{2\overline{\lambda\rho}}\right)\mathrm{d}V$$

or:

$$U_0 = U - \alpha_R\Theta U + \frac{\alpha_R U^3}{24\overline{\lambda\rho}} = U\left(1-\frac{2}{3}\alpha_R\Theta\right) \tag{41}$$

For $\alpha_R\Theta \approx 1$ this can be written as:

 doi:10.20944/preprints202403.1416.v1

$$\frac{U}{U_0} = \frac{1}{1 - \frac{2}{3}\alpha_R \Theta} \approx 1 + \frac{2}{3}\alpha_R \Theta \tag{42}$$

Since the current tube of both strictions is traveled by the same current intensity, it can be written:

$$\frac{U}{U_0} = \frac{R_\Theta}{R_0} = 1 + \frac{2}{3}\alpha_R \Theta \tag{43}$$

and finally:

$$R_\Theta = R_0 \left(1 + \frac{2}{3}\alpha_R \Theta\right) \tag{44}$$

It can therefore be concluded that the resistance of the heated contact can be calculated, starting from the resistance of the unheated contact, with a dependence relationship similar to resistors, in which the temperature coefficient of the resistance is 2/3 of the temperature coefficient of the resistivity.

The Thomson effect refers to the case when an electric current of intensity i travels through a conductor along which there is a temperature gradient, and additional power develops inside the conductor:

$$P_T = \pm k_T \cdot \Delta T \cdot i \tag{45}$$

where k_T is the Thomson coefficient and ΔT is the temperature difference on the conductor.

The sign ± depends on the direction of current relative to the direction of the temperature gradient. The + sign is considered if the current travels through the conductor in the same direction as the gradient. Current travels through one contact element once in the same direction as the gradient and in the other element in the opposite direction, as shown in Figure 10. As a result, one contact element heats up additionally, and the other cools down. These phenomena manifest themselves in the touch zone, where the temperature is the highest. Accordingly, the anode will be warmer than the cathode.

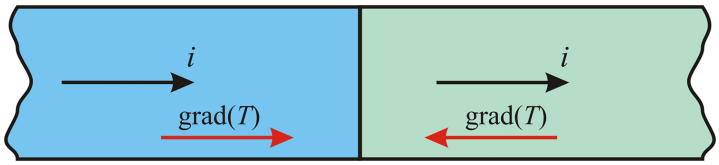

Figure 10. Current travel and the Thomson effect in a contact.

3. Modeling and Simulation of the Electrical Contacts Using Numerical Methods

We have shown in Section 2 that between the absolute temperature of the contacts and their potential there is a dependence expressed by Equation (28). This equation has a theoretical character, and its integration through analytical methods is difficult. For this reason, the dependence between the potential and temperature of an electrical contact will be analyzed by numerical methods with the aid of the COMSOL Multiphysics software.

3.1. Geometry of the Model

The model of the electrical contact, consisting in an assembly of two contact elements as shown in Figure 11, was built using SolidWorks software. The two elements are identical and the material from which they are built is copper. The geometry and dimensions of one contact element are shown in Figure 12. The advantage of using SolidWorks for the build of the model is given by the dynamic

 doi:10.20944/preprints202403.1416.v1

live link feature it has with COMSOL, meaning that any change to the geometry that is done in SolidWorks, is automatically imported into the COMSOL Multiphysics simulation model.

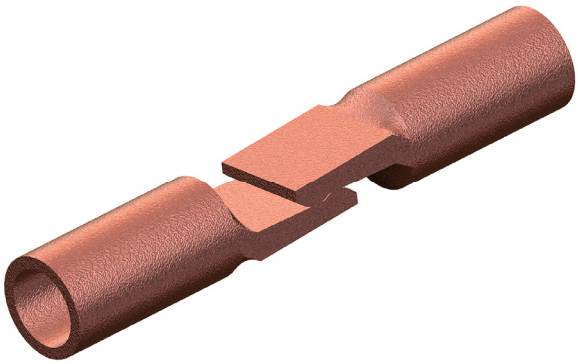

Figure 11. The model of the electrical contact.

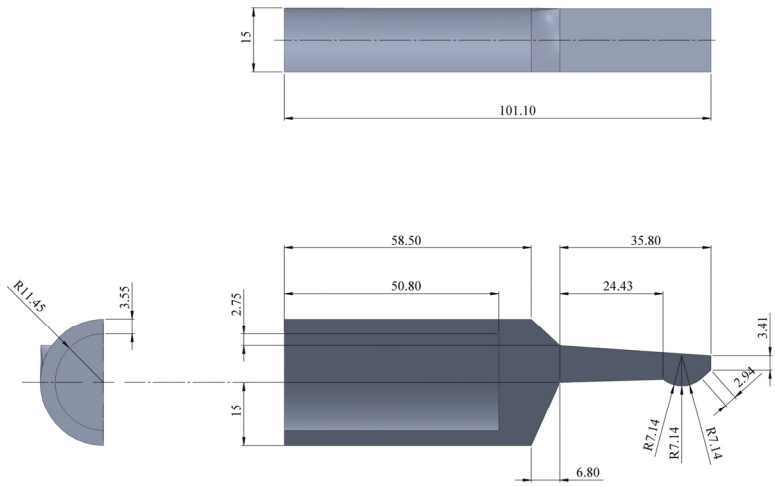

Figure 12. Geometry and dimensions of one contact element.

3.2. The Step-by-Step Simulation Setup for Comsol

The simulation was performed for a 3D model in two distinct steps within stationary studies of Structural Mechanics>Solid Mechanics (solid) and Heat Transfer>Electromagnetic Heating>Joule Heating type.

The two contact elements presented above have a cylindrical body with the touching ends shaped similar to a hook. Here the coupling of apparent thermal and electrical resistances by means of mechanical contact pressure takes place. It was considered that the initial temperature of the contact is equal to the ambient temperature, and the difference of electric potential between the contact elements produces heating by Joule effect. Figure 13 shows the geometry of the imported model into COMSOL. In the Definitions menu the Contact Pair type was chosen for the contact elements and their Source Boundaries and Destination Boundaries were defined as shown in Figure 14. Next, for the entire model the material (copper) was chosen with its predefined characteristics from the library as can be seen in Figure 15. The fixed surfaces have been established as shown in Figure 16. These surfaces represent the inner part of the semi-cylindrical areas of the contacts. Since the imported geometric pattern is a cross section through the two electrical contacts, we used the Boundary>Symmetry option from the Physics menu, thus the plane of symmetry of the model has been defined (Figure 17). This approach simplifies computations for half of the model.

 doi:10.20944/preprints202403.1416.v1

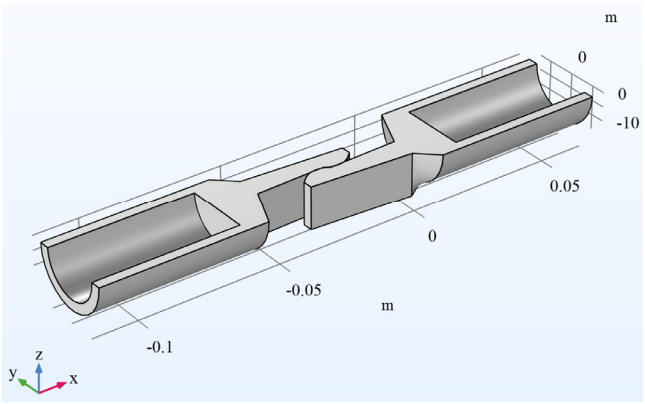

Figure 13. The model geometry as imported into COMSOL.

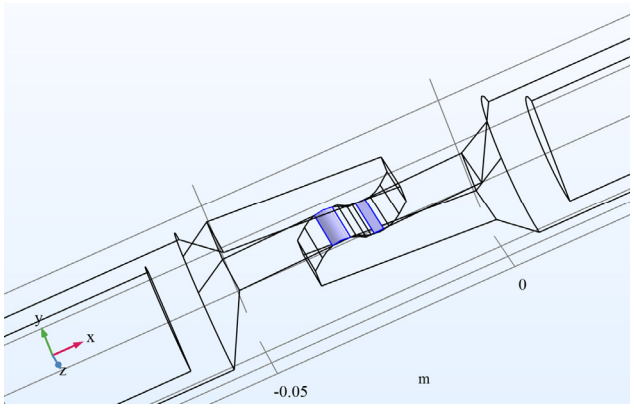

Figure 14. The contact elements, source and destination boundaries definition in COMSOL.

Material Contents

Property	Variable	Value	Unit	Property group
Electrical conductivity	sigma_iso ; sigmaii = sigma_iso,...	5.998e7[S/m]	S/m	Basic
Heat capacity at constant pressure	Cp	385[J/(kg*K)]	J/(kg·K)	Basic
Relative permittivity	epsilonr_iso ; epsilonrii = epsilon...	1	1	Basic
Density	rho	8960[kg/m^3]	kg/m³	Basic
Thermal conductivity	k_iso ; kii = k_iso, kij = 0	400[W/(m*K)]	W/(m·K)	Basic
Young's modulus	E	110e9[Pa]	Pa	Young's modulus and Poisson's ratio
Poisson's ratio	nu	0.35	1	Young's modulus and Poisson's ratio
Relative permeability	mur_iso ; murii = mur_iso, murij...	1	1	Basic
Coefficient of thermal expansion	alpha_iso ; alphaii = alpha_iso, a...	17e-6[1/K]	1/K	Basic
Reference resistivity	rho0	1.72e-8[ohm*m]	Ω·m	Linearized resistivity
Resistivity temperature coefficient	alpha	0.0039[1/K]	1/K	Linearized resistivity
Reference temperature	Tref	298[K]	K	Linearized resistivity

Figure 15. The material and its predefined characteristics chosen from the material library.

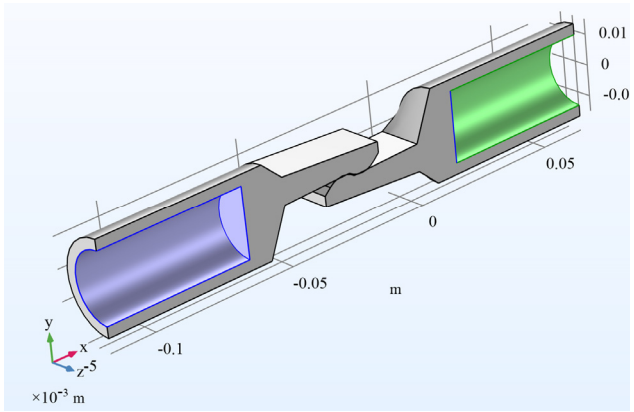

Preprints.org (www.preprints.org) | NOT PEER-REVIEWED | Posted: 25 March 2024 doi:10.20944/preprints202403.1416.v1

Figure 16. Fixed surfaces definition.

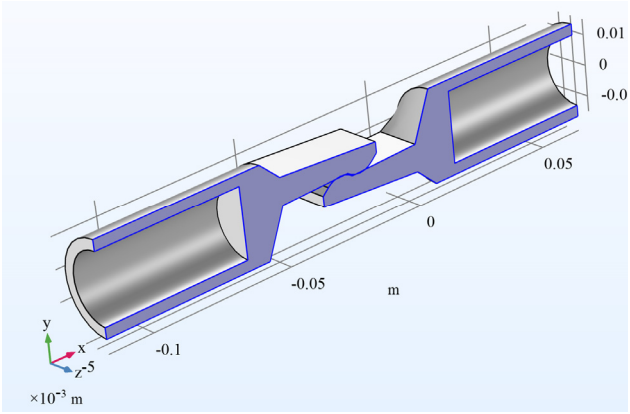

Figure 17. The plane of symmetry for the model.

The contact method was chosen of Augmented Lagrangian type with the initial value of the contact pressure T_n = 1×10^7 N/m^2. Regarding the heat transfer it was picked as Convective heat flux type with a heat transfer coefficient h = 2. The difference of electric potential representing the voltage drop on the simulated contact was imposed by assigning zero voltage (Ground) to the base surface of the cylinder to one of the contact elements, and a voltage of 1 mV (Electric Potential) to the other contact element, as shown in Figures 18a,b.

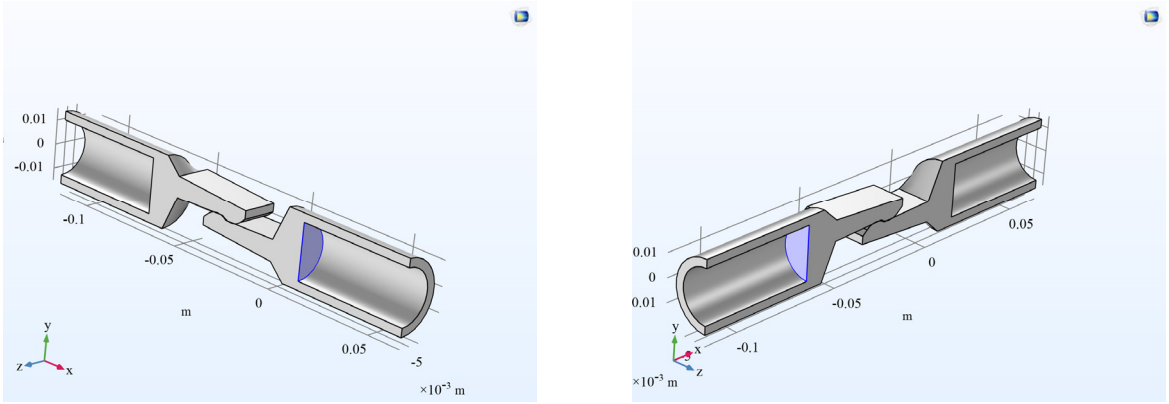

(**a**) (**b**)

Figure 18. (**a**). Contact element with Zero voltage (Ground). (**b**). Contact element with 1 mV voltage (Electric Potential).

The finite element mesh is of the Free Tetrahedral type, and the model after meshing looks like shown in Figure 19.

 doi:10.20944/preprints202403.1416.v1

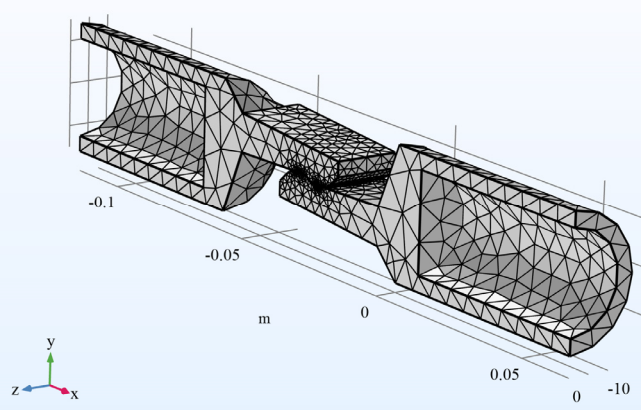

Figure 19. The contact model after finite element meshing.

As stated at the start of 3.2 subsection, the simulation is carried out in two stages. In the first stage, only solid mechanics phenomena are simulated using the Solid Mechanics (solids) solver as shown in Figure 20, and in the second stage the Joule effect and heat transfer phenomena are simulated using the Electric Currents and Heat Transfer in Solids solvers as shown in Figure 21. The two stages simulation follows the need to first solve the effect of the contact pressure on the characteristics of the electrical contact elements material, and only next the Joule effect of the contacts and its effect are evaluated.

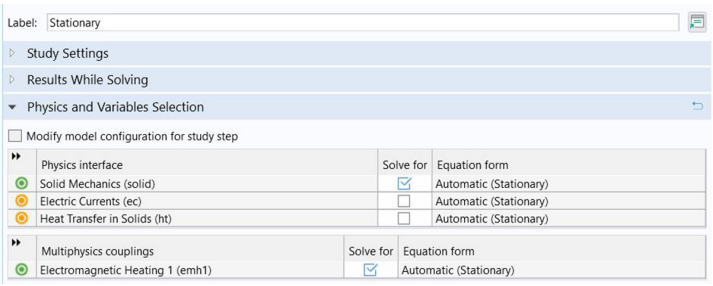

Figure 20. Simulation of the solid mechanics phenomena.

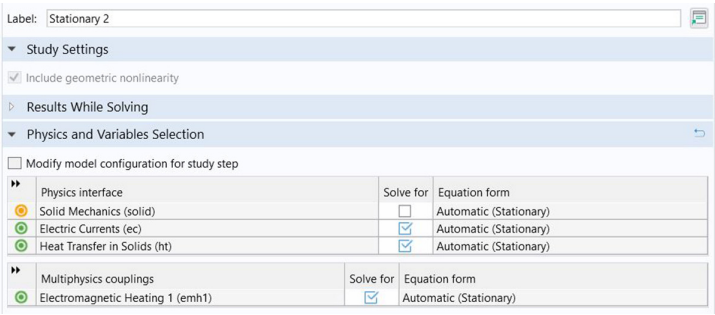

Figure 21. Simulation of the Joule effect and heat transfer phenomena.

The simulation of the temperature variation when the current flows through the current path of the contact is done considering the initial temperature of the contact elements T = 293.15 K. The base values of the parameters for the contact elements were setup prior to simulation. Thus, in the Solid Mechanics module of Contact Pair 1, the contact pressure was set to $T_n = 1 \times 10^7$ N/m^2. In the Electric Currents >Pair Electrical Contact module, for the same Contact Pair 1 the Microhardness parameter

 doi:10.20944/preprints202403.1416.v1

had an assigned value of H_c = 0.1 GPa. In the Heat Transfer in Solids module, an identical value of the microhardness was set for the Thermal Contact pair.

4. Simulation Results and Discussion

4.1. Results of the Mechanical Simulation

By running the simulation, it is observed that there is an increase in the von Mises stress (Figure 22) in the contact where the contact point and the current path are located. A detailed view of the shape of the von Mises stress can be observed in Figure 23. By analyzing this figure, it is visible that the increase of von Mises stress concentrates to the area of physical contact points between the contact elements.

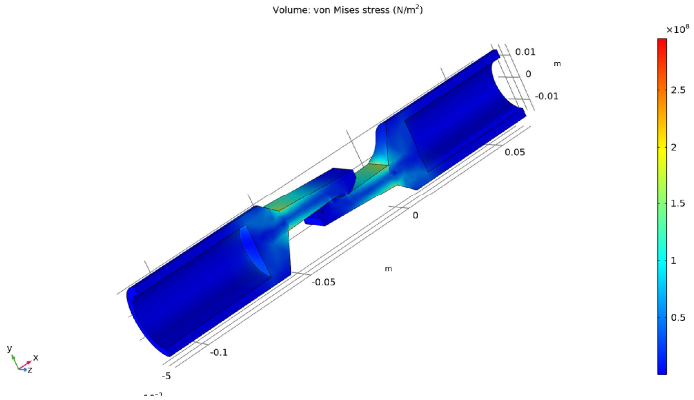

Figure 22. The von Mises stress in the contact.

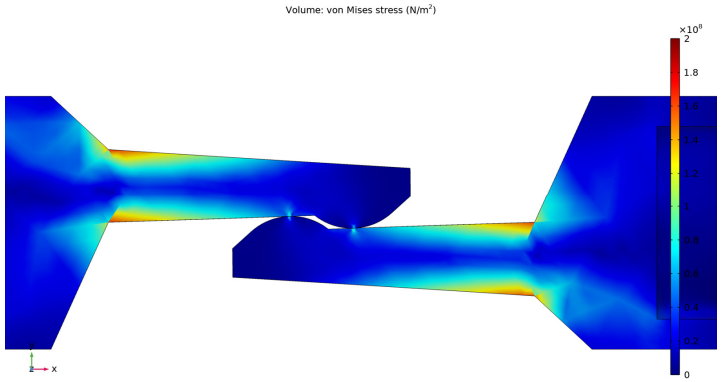

Figure 23. Details of the shape of von Misses stress at the contact point and current path location.

Figure 24 shows the contact force resulting from the simulation and Figures 25 and 26 shows the detailed variation of this force.

Preprints.org (www.preprints.org) | NOT PEER-REVIEWED | Posted: 25 March 2024 doi:10.20944/preprints202403.1416.v1

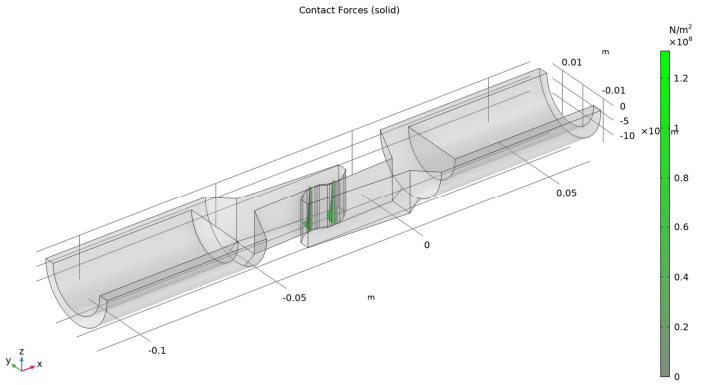

Figure 24. The contact forces (three-dimensional view).

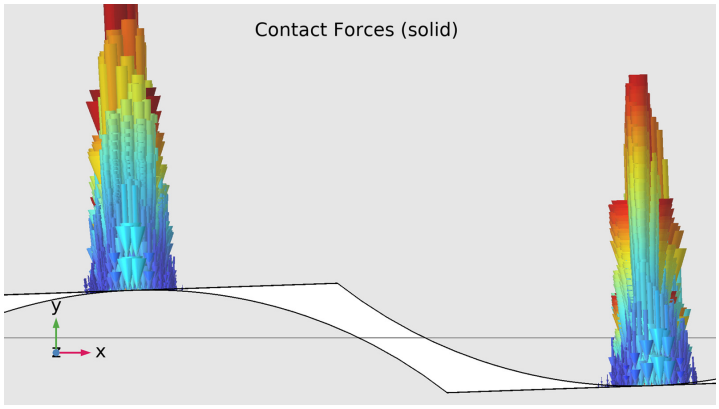

Figure 25. The contact forces (detailed representation).

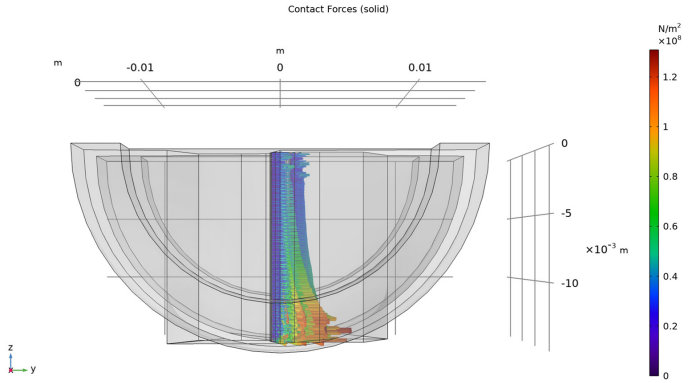

Figure 26. The contact forces in orthographic projection.

4.2. Results of the Electro-Thermal Simulation

The variation in the electrical potential on the current path of the contact is shown in Figure 27. As expected, it varies between 0 V, which corresponds to the right-side element of the contact which is grounded, and 3 mV on the left side-element. The difference of electric potential is actually the voltage drop on the elements of the electrical contact.

 doi:10.20944/preprints202403.1416.v1

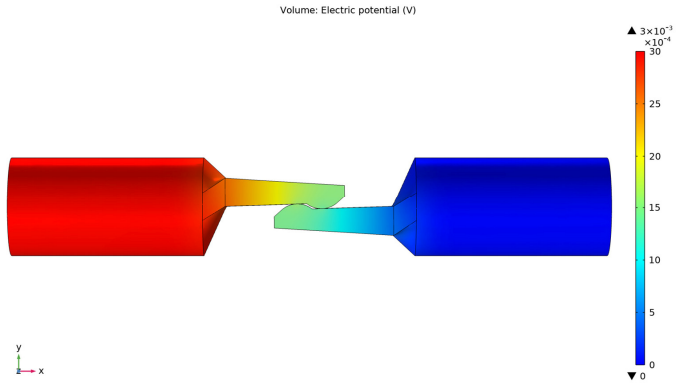

Figure 27. The electrical potential of the contact along the current path.

The variation of the electric field amplitude along the current path is shown in Figure 28. The Multislice mode combined with the Streamline Multislice mode was used for this representation. Figure 29 shows a detail of the variation of the electric field amplitude in the touching area of the contact elements.

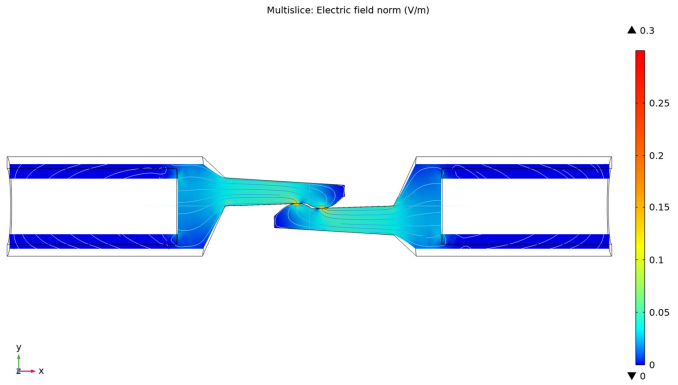

Figure 28. The variation of the electric field amplitude.

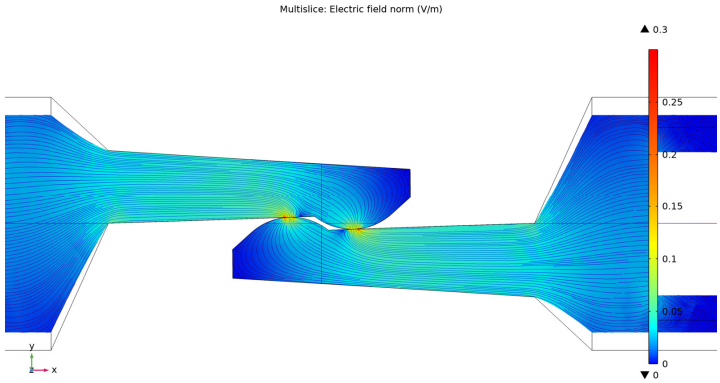

Figure 29. Detailed view of the variation of the electric field amplitude at the touching area.

The variation of temperature on the current path following the simulation is visible in Figure 30, where one can observe that the highest temperature is in the touching area of the electrical contact.

 doi:10.20944/preprints202403.1416.v1

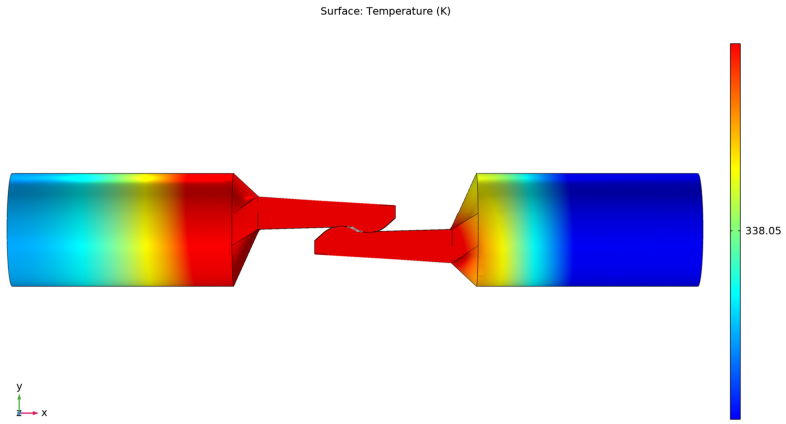

Figure 30. The variation of temperature on the current path and contact surface.

Figure 31 shows the simulation results related to the temperature gradient variation along a cut plane passing through the axis of the current path and parallel to plane XY. It can be seen both from the representation of the magnitude of this quantity <K/m> and from the streamline representation, that the heat transfer from the element of contact with zero electrical potential is greater than that corresponding to the element of contact with an electric potential of 3 mV.

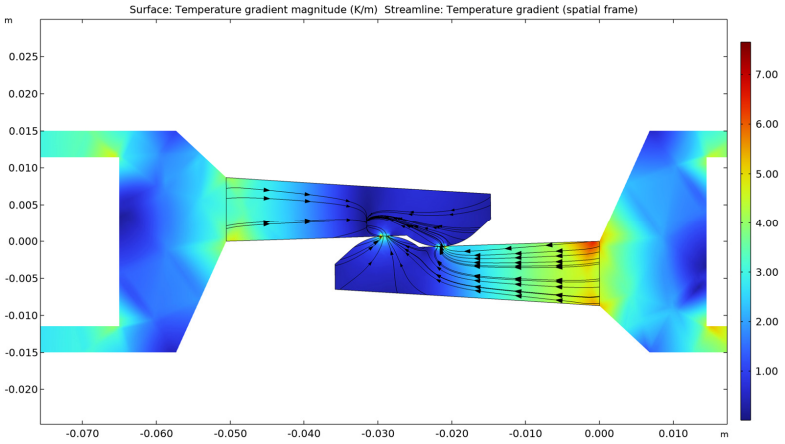

Figure 31. The temperature gradient variation along a cutting plane.

Figure 32 shows the spatial variation of the current path temperature gradient.

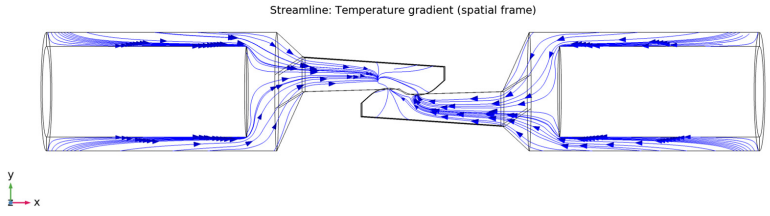

Figure 32. The spatial variation of the temperature gradient along the current path.

Figure 33 shows the variation in the current path temperature by isothermal contours. Isothermal surfaces were drawn for 15 temperature levels. Figure 34 shows the temperature variation of the two contact elements and the variation of the current density on a surface that passes through the axis of symmetry of the current path and is parallel to plane XY, using streamline representation.

Preprints.org (www.preprints.org) | NOT PEER-REVIEWED | Posted: 25 March 2024 doi:10.20944/preprints202403.1416.v1

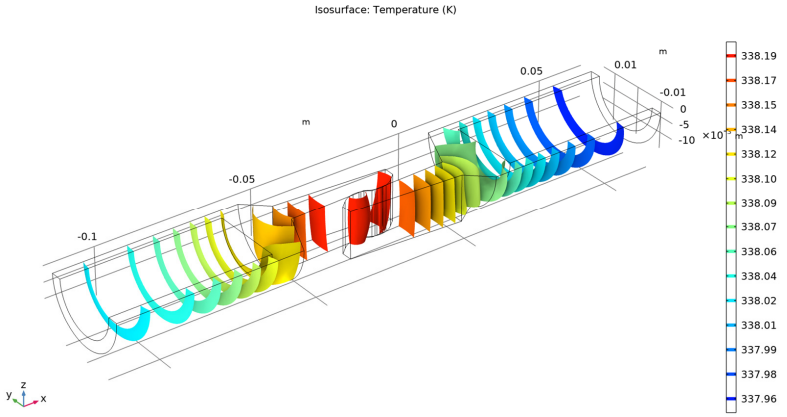

Figure 33. Current path temperature represented by isothermal contours.

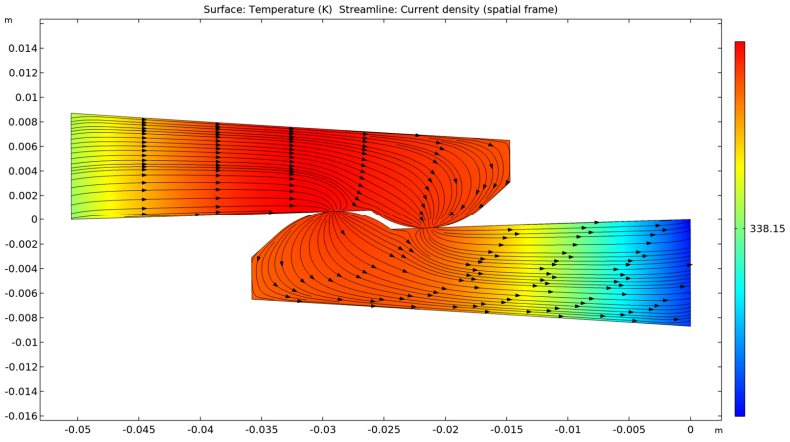

Figure 34. Temperature variation of the contact and the current density using streamlines.

A cut plane was built as shown in Figure 35a, parallel to plane XZ and passing through the origin of the cartesian coordinate system (Y=0). Figure 35b,c show the details regarding the positioning of this cut plane.

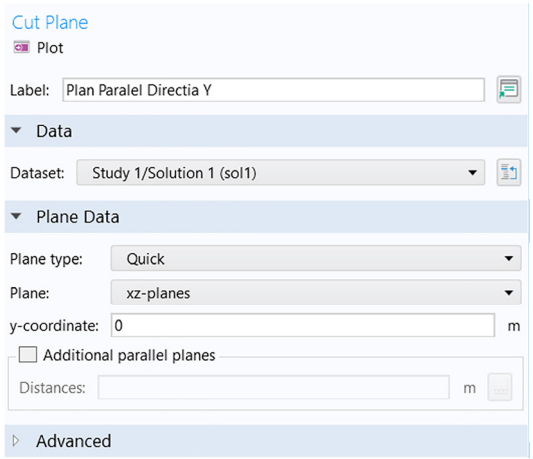

(**a**). Cut plane building parameters

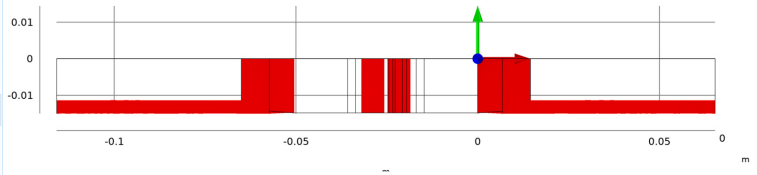

(**b**). Cut plane top view

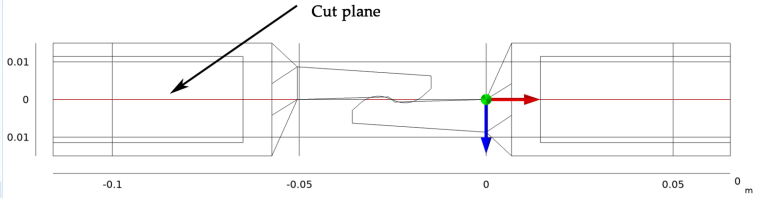

(**c**). Cut plane side view

Figure 35. Cut plane building and details on its positioning.

doi:10.20944/preprints202403.1416.v1

 doi:10.20944/preprints202403.1416.v1

In Figure 36 the variation of the current density on the cut plane defined above is presented. In Figure 37 the variation of the current density is shown using a 3-dimensional representation, and the Max/Min-Point diagram showing the density of electric energy. One can notice that the highest density of electric energy is at the touching area of the contact elements.

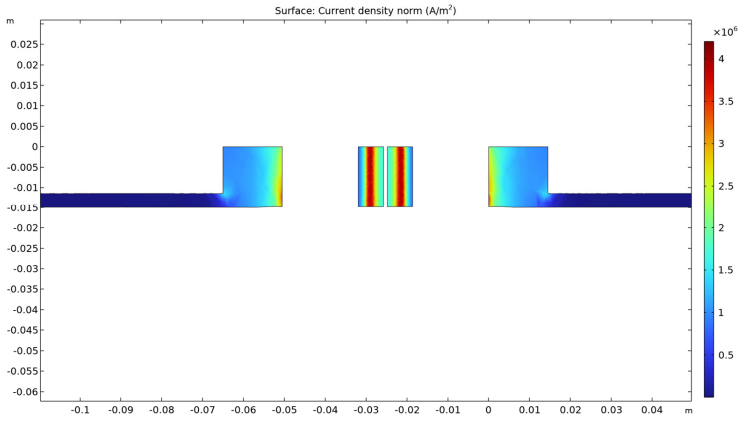

Figure 36. Variation of the current density on the cut plane. 105.

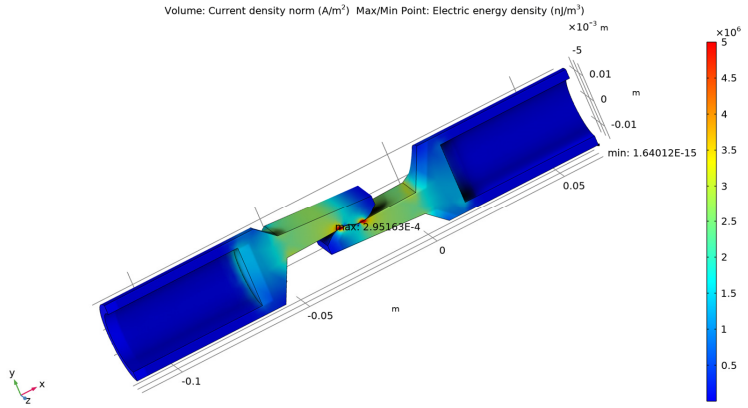

Figure 37. Variation of the current density in the contact (3D), and the Max/Min-Point diagram of the electric energy density.

A dataset element of the type Edge 3D was created (see in Figure 38) along an edge line of one contact element, in order to plot the temperature variation along this edge as presented in Figure 39.

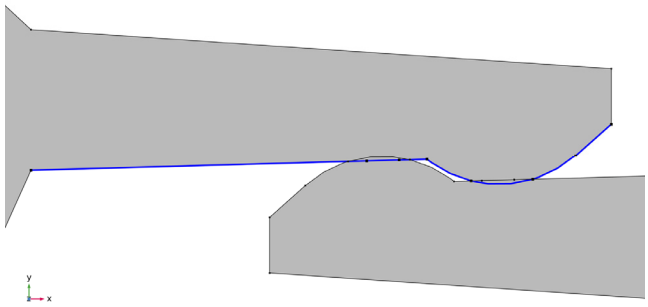

Figure 38. Edge 3D type dataset created for the edge of a contact element.

 doi:10.20944/preprints202403.1416.v1

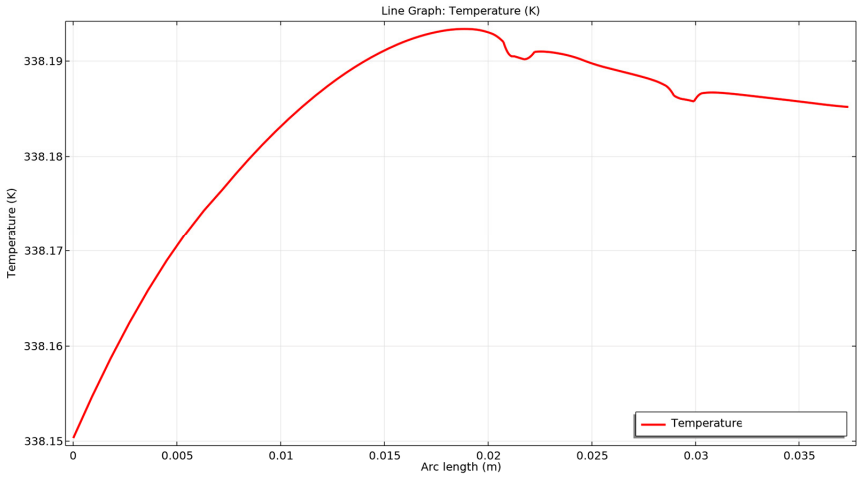

Figure 39. Variation of the temperature along the contact element edge.

In a similar way, two Edge 3D type datasets are created (Figure 40a,b) for the contours of both electrical contact elements, to be used for the plotting of the variation graph of the electrical potential, as shown in Figure 42.

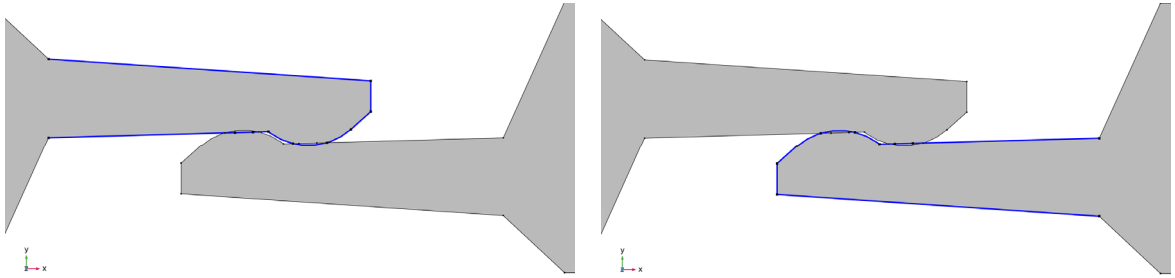

(a). (b).

Figure 40. The two Edge 3D datasets created for the contours of both electrical contact elements.

doi:10.20944/preprints202403.1416.v1

 doi:10.20944/preprints202403.1416.v1

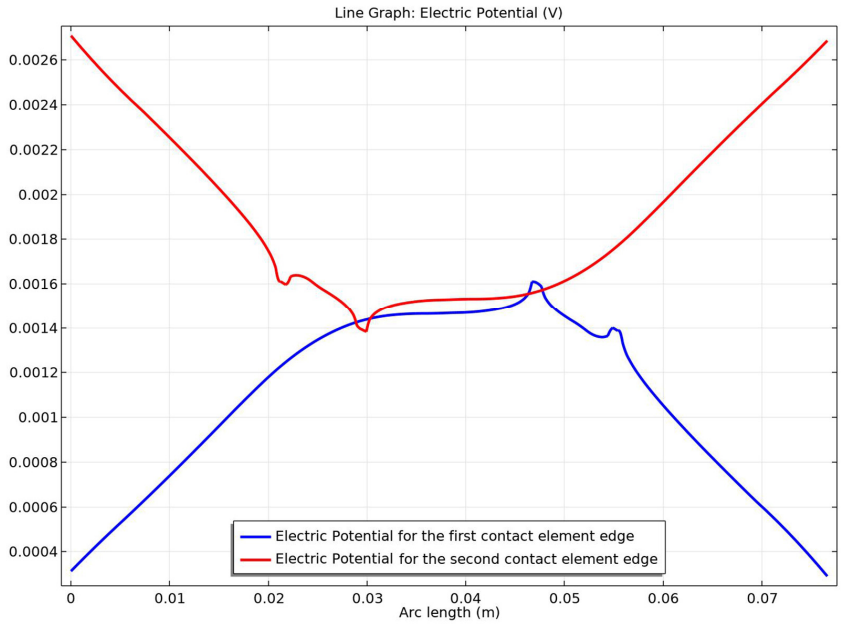

Figure 41. Variation of the electric potential along the two contact element edges.

In order to highlight the variation of the maximum temperature of the current path and its dependence on the value of the contact voltage, the simulations were run for various values of the potential difference between the two elements of the electrical contact. This data along this and the values of the maximum temperature, and the values of the temperature increase as compared to the ambient temperature are all summarized in Table. 1.

Table 1. Temperature increase function of the contact voltage as resulted from simulations.

Electric potential (contact voltage) difference [V]	Maximum contact temperature [K]	Temperature increase [ΔT]
Ambient temperature T = 293.15 K		
0	293.15	0.00
0.50	294.28	1.13
1.00	298.07	4.92
2.00	312.93	19.78
3.00	337.65	44.50
4.00	372.39	79.25
5.00	416.96	123.81

This variation of the temperature as a function of the contact voltage values is plotted in Figure 42. As one can observe, the red curve representing this variation has a parabolic shape. A trendline curve of polynomial type 2 represented in black color was also traced with its equation displayed. This trendline overlaps the curve of the variation of the temperature increase.

 doi:10.20944/preprints202403.1416.v1

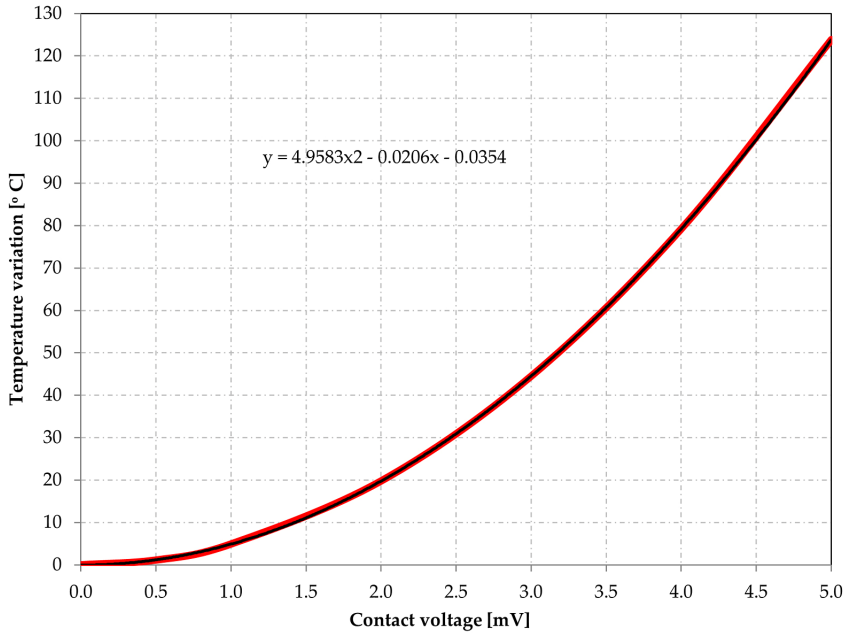

Figure 42. Variation of the temperature as function of the contact voltage.

5. Conclusions

The present paper studies and highlights—using numerical methods of modeling and simulation—the dependence between the contact voltage (the voltage drop on the contact) and the variation of its temperature, but also of the current path within the contact. The study was carried using COMSOL Multiphysics software, specifically three of its simulation modules: solid state mechanics module, electric current module and heat transfer module. The geometric model was build using SolidWorks and imported into COMSOL using the real-time link, which allows for easy modification of the model geometry for other modeling and simulation approaches. The results obtained after the simulations were computed, highlighted the following:

- The von Misses stress has higher values in the current path area where the flat part intersects with the cylindrical shape for each contact element, and also in the area of the physical touching of the two contact elements;
- The contact forces have maximum value at the contact points;
- The electric field amplitude along the current path and the contact elements is maximum at the touching point, where the transverse surface has a minimum value;
- The temperature gradient along the contact proves that the highest temperature is in the touching area of the electrical contact. The gradient also shows it is higher in the direction from the zero potential contact elements towards the contact point. This supports the theoretical aspects presented in the Introduction section and shown in Figure 10.
- The variation of temperature in the current path and the contact elements was graphically represented by isothermal surfaces for 15 temperature levels;
- The dependence between the temperature variation of the two contact elements and the variation of the current density was shown using color legend, on a plane that passes through the axis of symmetry of the current path and is parallel to plane XY, and also using streamline representation;
- In order to have a more conclusive picture of the current density, we presented its variation on the surface of a horizontal longitudinal cut plane;
- By drawing the temperature variation diagram along the edges of the contacts, it was observed that its maximum value is found at the touching points of the contact elements takes place;

- The maximum contact temperature values were computed by simulation for contact voltages between 0 and 5 mV. Thus, the curve of variation of the increase in contact temperature relative to the contact temperature was plotted, finding this variation as parabolic

The study of the obtained values during simulations, indicates an undesirable increase in contact temperature for values higher than 4 mV of voltage drop, with temperatures that may affect the integrity of insulating materials in the electrical contact. This finding is important as damage to the insulation materials may cause the phenomenon of overturning or short circuit in the electrical contact devices, thus leading to fire and damage, aspects that can constitute a future direction of research.

Author Contributions: All authors have contributed to the preparation of this manuscript. Conceptualization, A.A., F.D.P., and D.P.; methodology, S.M.R., A.A., I.B., and M.A.R.; software, F.D.P., A.A, and D.P.(F).; writing—original draft preparation, S.M.R., F.D.P., and A.A.; writing—review and editing, D.P., M.A.R., I.B., and D.P.(F). All authors have read and agreed to the published version of the manuscript.

Funding: This research received no external funding.

Institutional Review Board Statement: Not applicable.

Informed Consent Statement: Not applicable.

Data Availability Statement: Not applicable.

Conflicts of Interest: The authors declare no conflict of interest.

References

1. Johnson, K.L. *Contact mechanics*. Cambridge University Press: Cambridge, UK, 1985. https://doi.org/10.1017/CBO9781139171731
2. Braunovic, M.; Myshkin, N.K.; Konchits, V. *Electrical Contacts: Fundamentals, Applications and Technology*; CRC Press: Boca Raton, US, 2006. https://doi.org/10.1201/9780849391088
3. Popov, V.L. *Contact Mechanics and Friction*; Springer-Verlag: Germany, 2017. https://doi.org/10.1007/978-3-662-53081-8_1
4. Slade, P.G. *Electrical Contacts: Principles and Applications*, 2nd ed.; CRC Press: London, UK, 2017. https://doi.org/10.1201/b15640
5. Barber, J.R. *Contact Mechanics*, 1st ed.; Springer: Berlin, Germany, 2018.
6. Zhou, X. Electric Contact, Elements, and Systems. In *Encyclopedia of Tribology*, Wang, Q.J., Chung, Y.W., Eds. Springer: Boston, MA, USA, 2013. https://doi.org/10.1007/978-0-387-92897-5_386
7. Persson, B.N.J. On the Electric Contact Resistance. *Tribology Letters* **2022**, *70*, 88. https://doi.org/10.1007/s11249-022-01630-2
8. Müser, M.H.; Wang, A. Contact-patch-size distribution and limits of self-affinity in contacts between randomly rough surfaces. *Lubricants* **2018**, *6*, 85. https://doi.org/10.3390/lubricants6040085
9. Prodanov, N.; Dapp, W.B.; Müser, M.H. On the contact area and mean gap of rough, elastic contacts: dimensional analysis, numerical corrections, and reference data. *Tribology Letters* **2014**, *53*, 433. https://doi.org/10.1007/s11249-013-0282-z
10. Qiu, D.; Peng, L.; Yi, P.; Lai, X. A micro contact model for electrical contact resistance prediction between roughness surface and carbon fiber paper. *Int. J. Mech. Sci.* **2017**, *124*, 37–47. https://doi.org/10.1016/j.ijmecsci.2017.02.026
11. He, L.P.; Cai, Z.B.; Peng, J.F.; Deng, W.L.; Li, Y.; Yang, L.Y.; Zhu, M.H. Effects of oxidation layer and roughness on the fretting wear behavior of copper under electrical contact. *Materials Research Express* **2020**, *6(12)*, 1265e3. https://doi.org/10.1088/2053-1591/ab5aaf
12. Zhang, C.; Ren, W.; Liao, X. On the Relationship between Contact Resistance and Load Force for Electrode Materials with Rough Surfaces. *Materials* 2022, *15*, 5667. https://doi.org/10.3390/ma15165667
13. Biele, L.; Schaaf, P.; Schmid, F. Influence of Contact Pressure on the Specific Electrical Contact Resistance of Copper. *IEEE Transactions on Components, Packaging and Manufacturing Technology* **2022**, *12*, 973-980. https://doi.org/10.1109/tcpmt.2022.3176740
14. Timsit, R.S. Electrical Contacts: Scientific Fundamentals. In *Encyclopedia of Tribology*, Wang, Q.J., Chung, Y.W., Eds. Springer: Boston, MA, USA, 2013. https://doi.org/10.1007/978-0-387-92897-5_429
15. Faltin, C. Exact solution of constriction resistance and temperature field within a homogeneous cylindrical body heated by an isothermal circular contact spot. *International Communications in Heat and Mass Transfer* **1985,** 12(6), 677–86. https://doi.org/10.1016/0735-1933(85)90020-x.34

16. Negus, K.J.; Yovanovich, M.M.; Beck, J.V. On the nondimensionalization of constriction resistance for semi-infinite heat flux tubes. *Journal of Heat Transfer* **1989**, *111(3)*, 804–7. https://doi.org/10.1115/1.3250755.35
17. Yovanovich, M.M. Overall constriction resistance between contacting rough, wavy surfaces. *International Journal of Heat and Mass Transfer* **1969**, *12*, 1517-20. https://doi.org/10.1016/0017-9310(69)90031-3.36
18. Lambert MA, Fletcher LS. Thermal contact conductance of spherical rough metals. *Journal of Heat Transfer* **1997**, *119(4)*, 684–90. https://doi.org/10.1115/1.2824172.37
19. Lei, H.; Zhu, X.; Wang, H.; Chen, J.; Liu, Q.; Niu, C.; Wang, L.; Yang, F. Investigation on Mathematical Model of Electric Contact Based on Fractal Geometry. *Lecture Notes in Electrical Engineering*, 2021, 617–628. https://doi.org/10.1007/978-981-33-6606-0_56
20. Capelli, F.; Riba, J. -R.; Rupérez, E.; Sanllehí, J. A Genetic-Algorithm-Optimized Fractal Model to Predict the Constriction Resistance From Surface Roughness Measurements. *IEEE Transactions on Instrumentation and Measurement* **2017**, *66(9)*, 2437-47. https://doi.org/10.1109/TIM.2017.2707938
21. Zou, M.; Yu, B.; Cai, J.; Xu, P. Fractal model for thermal contact conductance. *Journal of Heat Transfer* **2008**, *130*(10), 101301. https://doi.org/10.1115/1.2953304
22. Talukder, S.; Yeo, C.-D.; Hong, Y.-K.; Choi, M.; Flicek, R.C.; Bishop, J.E. Analytical modeling and simulation of electrical contact resistance for elastic rough electrode surface contact including frictional temperature rise. *AIP Advances* **2022**, *12 (2)*, 025204. https://doi.org/10.1063/5.0073093
23. Popescu, A.; Lazarescu, E.; Frigura-Iliasa, F.M.; Dolga, L.; Filipescu, H.E.; Andreea, A. Analytical Model for the Electrodynamical Forces inside Electrical Contacts of Commutation Devices. In 2019 20th International Scientific Conference on Electric Power Engineering (EPE), Kouty nad Desnou, Czech Republic, 2019, pp. 1-4. https://doi.org/10.1109/EPE.2019.8778079.
24. Shah, S.G.; Krithivasan, V.; Jackson, R.L. An electro-mechanical contact analysis of a three-dimensional sinusoidal surface against a rigid flat. *Wear* ***2011***, *270*, 914-21. https://doi.org/10.1016/j.wear.2011.03.001
25. Blauth, M.; Berger, F; Song, J. Analytical and Experimental Investigation of the Electrical-Thermal Behaviour of Electrical Contact Systems. *British Journal of Applied Science & Technology* **2014**, *4*(1), pp.18-39. https://doi.org/10.9734/bjast/2014/5536
26. Dutta, S.; Vikram, G.N.V.R.; Bobji, M.S.; Mohan, S. Table top experimental setup for electrical contact resistance measurement during indentation. *Measurement* **2020**, *152*, p.107286
27. Kogut, L.; Komvopoulos, K. Analysis of interfacial adhesion based on electrical contact resistance measurements. *Journal of applied physics* **2003**, *94*(10), 6386-6390.
28. Beloufa, A. Numerical and experimental optimization of mechanical stress, contact temperature and electrical contact resistance of power automotive connector. *International Journal of Mechanics* **2010**, *4*(4), 94-104.
29. Zhang, S.; Zhao, X.; Ye, M.; He, Y. Theoretical and Experimental Study on Electrical Contact Resistance of Metal Bolt Joints. *IEEE Transactions on Components, Packaging and Manufacturing Technology* **2019**, *9*, 1301-1309. https://doi.org/10.1109/TCPMT.2019.2920854
30. Pradille, C.; Bay, F.; Mocellin, K. An Experimental Study to Determine Electrical Contact Resistance. In Proceedings of the 56th IEEE Holm Conference on Electrical Contacts, Charleston, SC, USA, 2010, pp. 1-5. https://doi.org/ 10.1109/HOLM.2010.5619522
31. Wangwiwattana, S.; Yoshikazu, K. Joule Heating and Arc-Fault-Induced Electrical Fires for Commercial-Grade Copper and Brass in Low-Voltage Electrical Systems. *Appl. Sci.* **2022**, *12*, 4710. https://doi.org/10.3390/app12094710
32. Zavarise, G.; Wriggers, P.; Stein, E.; Schrefler, B. A. Real contact mechanisms and finite element formulation—a coupled thermomechanical approach. *International Journal for Numerical Methods in Engineering* **1992**, *35*(4), 767–785. https://doi.org/10.1002/nme.1620350409
33. Wriggers, P.; Miehe, C. Contact constraints within coupled thermomechanical analysis-a finite element model. *Computer Methods in Applied Mechanics and Engineering* **1994**, *113*, 301–319. https://doi.org/10.1016/0045-7825(94)90051-5
34. Zienkiewicz, O.C.; Taylor, R.L. *The finite element method*, 4th ed., McGraw-Hill: London, UK, 1989.
35. Agelet de Saracibar, C. Numerical analysis of coupled thermomechanical frictional contact problems. Computational model and applications. *Archives of Computational Methods in Engineering* **1998**, *5*(3), 243–301. https://doi.org/10.1007/bf02897875
36. Weißenfels, C.; Wriggers, P. Numerical modeling of electrical contacts. *Computational Mechanics* **2010**, *46*, 301–314. https://doi.org/10.1007/s00466-009-0454-8
37. Renouf, M.; Fillot, N. Coupling electrical and mechanical effects in discrete element simulations. *International Journal for Numerical Methods in Engineering* **2007**, *74*(2), 238-254. https://doi.org/10.1002/nme.2157
38. Bourbatache, K.; Guessasma, M.; Bellenger, E.; Bourny, V.; Tekaya, A. Discrete modelling of electrical transfer in multi-contact systems. *Granular Matter* **2012**, *14*, 1–10. https://doi.org/10.1007/s10035-011-0307-y

39. Zhang, J.; Zavaliangos, A. Discrete element simulation of transient thermo-electrical phenomena in particulate system. In: Granular Material-Based Technologies, MRS Proceedings, Boston, MA, USA, vol. 759, 2002.
40. Fortin, J.; Millet, O.; De Saxcè, G. Numerical simulation of granular materials by an improved discrete element method. *International Journal for Numerical Methods in Engineering* **2004**, 62, 639–663. https://doi.org/10.1002/nme.1209
41. Gwinner, J.; Stephan, E. P. BEM for Contact Problems. In: *Advanced Boundary Element Methods. Springer Series in Computational Mathematics*; Springer, Cham, 2018; vol 52, pp. 389–449. https://doi.org/10.1007/978-3-319-92001-6_11
42. Frérot, L.; Bonnet, M.; Molinari, J.-F.; Anciaux, G. A Fourier-accelerated volume integral method for elastoplastic contact. *Computer Methods in Applied Mechanics and Engineering* **2019**, *351*, 951–976. https://doi.org/10.1016/j.cma.2019.04.006
43. Xu, Y.; Jackson, R. L. Boundary element method (BEM) applied to the rough surface contact vs. BEM in computational mechanics. *Friction* **2018**, *7*(4), 359–371. https://doi.org/10.1007/s40544-018-0229-3
44. Szulborski, M.; Łapczyński, S.; Kolimas, Ł.; Zalewski, D. Transient Thermal Analysis of the Circuit Breaker Current Path with the Use of FEA Simulation. *Energies* **2021**, *14*, 2359. https://doi.org/10.3390/en14092359
45. Zhang, C.; Ren, W.; Wang, G. A. Finite Element Method to Investigate Electrical Contact Behaviors Considering Asperity Interactions. In 2020 IEEE 66th Holm Conference on Electrical Contacts and Intensive Course (HLM), San Antonio, TX, USA, 2020, pp. 98-104. https://doi.org/10.1109/hlm49214.2020.9307862
46. Riba, J.-R.; Mancini, A.-G.; Abomailek, C.; Capelli, F. A 3D-FEM-based model to predict the electrical constriction resistance of compressed contacts. *Measurement* **2018**, *114*, 44–50. https://doi.org/10.1016/j.measurement.2017.09.003
47. Li, Y.-H.; Shen, F.; Ke, L.-L. Multi-physics electrical contact analysis considering the electrical resistance and Joule heating. *International Journal of Solids and Structures* **2022**, *256*, 111975. https://doi.org/10.1016/j.ijsolstr.2022.111975
48. Shen, F.; Ke, L.-L. Numerical Study of Coupled Electrical-Thermal-Mechanical-Wear Behavior in Electrical Contacts. *Metals* **2021**, *11*, 955. https://doi.org/10.3390/met11060955
49. Gonzalo, S.R. Coupling of mechanical and electrical contact behavior of current carrying connections in finite element models. B.Sc. Thesis, Universidad de Valladolid. Escuela de Ingenierías Industriales, Valladolid, Spain, 2021.
50. Angadi, S.V.; Jackson, R.L.; Pujar, V.V.; Tushar, M. A Comprehensive Review of the Finite Element Modeling of Electrical Connectors Including Their Contacts. *IEEE Transactions on Components, Packaging and Manufacturing Technology* **2020**, *10*, 836-844. https://doi.org/10.1109/TCPMT.2020.2982207.
51. Kim, S.H..; Lee, K.W. Numerical approach to joule heating analysis for electrical parts using MSC Marc. *Journal of Mechanical Science and Technology* **2015**, *29*, 2081–2087. https://doi.org/10.1007/s12206-015-0429-y.
52. Lv, B.; Zhou, S.J.; Zhao, L.Y.. Technical research on optimization design of contacts of electrical connector. *Journal of Zhejiang University-Science A* **2007**, *8*(3), 506–510. https://doi.org/10.1631/jzus.2007.A0506.
53. Duan, K.; Zhu, F.; Li, Y.; Tang, K.; Liu, S.; Chen, Y. Contact resistance investigation of electrical connector with different shrink range. In 2014 15th International Conference on Electronic Packaging Technology, Chengdu, China, 2014, pp. 1146–1149. https://doi.org/10.1109/ICEPT.2014.6922846.
54. Liu, H.; Leray, D.; Pons, P.; Colin, S. Finite element multi-physics modeling for ohmic contact of microswitches. In 15th International Conference on Thermal, Mechanical and Mulit-Physics Simulation and Experiments in Microelectronics and Microsystems (EuroSimE), Ghent, Belgium, 2014, pp. 1-8. https://doi.org/10.1109/EuroSimE.2014.6813877.
55. Angadi, S.V.; Wilson, W.E.; Jackson, R.L.; Flowers, G.; Rickett, B. A Multi-Physics Finite Element Model of an Electrical Connector Considering Rough Surface Contact. In 2008 IEEE 54th Holm Conference on Electrical Contacts, Orlando, FL, USA 2008, pp. 168-177. https://doi.org/10.1109/HOLM.2008.ECP.40.
56. Luo, S.; Wang, B.; Jiang, J.; Li, J.; Zou, G.; Zeng, L. Numerical analysis on mechanical and fatigue behaviors of aviation electrical connector considering structural effect. *International Journal of Numerical Modelling: Electronic Networks, Devices and Fields* **2024**, *37*(2), p.e3183. https://doi.org/10.1002/jnm.3183.
57. Ren, W.B.; Cui, L.; Zhai, G. Simulation of contacts inserted characteristics and contact resistance for electrical connector. *Journal of Electromechanical Components* **2012**, *32*(3), 40-48.
58. Terhorst, M.; Ozhoga-Maslovskaja, O.; Trauth, D.; Shirobokov, A.; Mattfeld, P.; Solf, M.; Klocke, F. Electro-thermo-mechanical contact model for bulk metal forming under application of electrical resistance heating. *The International Journal of Advanced Manufacturing Technology* **2017**, *89*, 3601-3618. https://doi.org/10.1007/s00170-016-9315-8.
59. Zhang, J.; Huang, L.; Chen, T.; Su, G. Simulation based analysis of electrical fire risks caused by poor electric contact between plug and receptacle. *Fire Safety Journal* **2021**, *126*, 103434. https://doi.org/10.1016/j.firesaf.2021.103434.

60. Guo, F.; Gu, X.; Li, L.; Wang, Z.; Wang, T.; Jia, S. Effect of surface microparameters on contact temperature of sliding electrical contact. *IEEE Transactions on Industrial Informatics* **2021**, *18*(9), pp. 5972-5981. https://doi.org./10.1109/TII.2021.3135426.
61. Zhang, C.; Zhao, Z.; Ren, W. Simulation and experimental investigation of contact spot temperature for electrical contact components. *IOP Conference Series: Materials Science and Engineering* **2021**, *1207*, 012021. https://doi.org/10.1088/1757-899X/1207/1/012021.
62. Andras, A.; Brînas, I.; Radu, S.M.; Popescu, F.D.; Popescu, V.; Budilica, D.I. Investigation of the Thermal Behaviour for the Disc-Pad Assembly of a Mine Hoist Brake Using COMSOL Multiphysics. *Acta Tech. Napoc. Ser. Appl. Math. Mech. Eng.* **2021**, *64*, 227–234.
63. Popescu, F.D.; Radu, S.M.; Andraș, A.; Brînaș, I.; Budilică, D.I.; Popescu, V. Comparative Analysis of Mine Shaft Hoisting Systems' Brake Temperature Using Finite Element Analysis (FEA). *Materials* **2022**, *15*, 3363. https://doi.org/10.3390/ma15093363.
64. Popescu, F.D.; Radu, S.M.; Andraş, A.; Brînaş, I.K. A Grafo-Numeric Method of Determination of the Operation Power of the Rotor of EsRc-1400 Bucket Wheel Excavator Using Computer Simulation in SolidWorks. *MATEC Web Conf.* **2019**, *290*, 04007. https://doi.org/10.1051/matecconf/201929004007.
65. Popescu, F.D.; Radu, S.M.; Andras, A.; Brinas, I.; Marita, M.-O.; Radu, M.A.; Brinas, C.L. Stability Assessment of the Dam of a Tailings Pond Using Computer Modeling—Case Study: Coroiești, Romania. *Appl. Sci.* **2024**, *14*, 268. https://doi.org/10.3390/app14010268.
66. COMSOL. *COMSOL Multiphysics 5.3. Reference Manual;* COMSOL AB: Stockholm, Sweden, 2017.
67. Zhai, C.; Hanaor, D.; Proust, G.; Gan, Y. Stress-dependent electrical contact resistance at fractal rough surfaces. *Journal of Engineering Mechanics* **2017**, *143(3)*, B4015001. https://doi.org/10.1061/(ASCE)EM.1943-7889.000096
68. Holm, R. *Electric Contacts: Theory and Application*; Springer Science & Business Media: New York, NY, USA, 2013.
69. Hortopan, G. *Aparate electrice. Principii și aplicații*; Editura Didactică și Pedagogică: București, Romania, 1980.